České vysoké učení technické v Praze
Fakulta jaderná a fyzikálně inženýrská
Katedra matematiky

Petr Pauš

Matematický model interakcí v diskrétní dislokační dynamice

Doktorský studijní program: Aplikace přírodních věd
Studijní obor: matematické inženýrství

Teze disertace k získání akademického titulu “doktor”, ve zkratce “Ph.D.”
Praha, říjen 2013

Disertační práce byla vypracována v kombinované formě doktorského studia na katedře matematiky Fakulty jaderné a fyzikálně inženýrské ČVUT v Praze.

Uchazeč: **Ing. Petr Pauš**
Katedra matematiky
Fakulta jaderná a fyzikálně inženýrská ČVUT v Praze
Trojanova 13
120 00 Praha 2

Školitel: **Prof. Dr. Ing. Michal Beneš**
Katedra matematiky
Fakulta jaderná a fyzikálně inženýrská ČVUT v Praze
Trojanova 13
120 00 Praha 2

Oponenti: **Prof. Robert F. Holub**
Center for Air Resources Engineering & Science
Clarkson University
Potsdam, NY 13699 USA

Prof. Ing. František Maršík, DrSc.
Ústav termomechaniky AV ČR
Dolejškova 1402/5, 182 00 Praha 8

Teze byly rozeslány dne: ....

Obhajoba disertace se koná dne .... v .... hod. před komisí pro obhajobu disertační práce ve studijním oboru matematické inženýrství v zasedací místnosti č. .... Fakulty jaderné a fyzikálné inženýrské ČVUT v Praze.

S disertací je možno se seznámit na děkanátě Fakulty jaderné a fyzikálně inženýrské ČVUT v Praze, na oddělení pro vědeckou a výzkumnou činnost, Břehová 7, Praha 1.

Prof. Ing. Miloslav Havlíček, DrSc.
předseda oborové rady pro studium
ve studijním oboru Matematické inženýrství
Fakulta jaderná a fyzikálně inženýrská ČVUT,
Břehová 7, Praha 1

Český překlad anglického názvu: **Matematický model interakcí v diskrétní dislokační dynamice**

Autor: Petr Pauš

Obor: Matematické inženýrství

Druh práce: Disertační práce

Vedoucí práce: Michal Beneš, Katedra matematiky, Fakulta jaderná a fyzikálně inženýrská, České vysoké učení technické v Praze

Konzultant: —

Abstrakt: Disertační práce se zabývá numerickou simulací dislokační dynamiky, interakcí dislokací a jejich topologickými změnami. Dislokace jsou reprezentovány parametrickým popisem rovinných křivek. Matematický model je založen na numerickém řešení rovnice, která popisuje pohyb křivky v závislosti na její křivosti. Největší pozornost je kladena na simulaci cross-slipu dislokací, kdy dislokace při svém pohybu změní skluzovou rovinu a vzájemně anihilují. Hlavním cílem je nalézt podmínky, při kterém ke cross-slipu dislokací dojde. Pohyb dislokací, jejich spojování a rozdělování a změna skluzové roviny jsou simulovány pomocí vylepšeného parametrického modelu. Vyšší numerická stabilita je dosažena redistribucí diskretizačních bodů podél křivky.

Klíčová slova: parciální diferenciální rovnice, metoda konečných diferencí, dislokační dynamika, cross-slip, anihilace

Title: **Mathematical model of interactions in discrete dislocation dynamics**

Author: Petr Pauš

Abstract: The thesis deals with the numerical simulation of dislocation dynamics, dislocation interaction, and changes in the dislocation topology (merging and splitting). The glide dislocations are represented by parametrically described curves moving in slip planes. The simulation model is based on the numerical solution of the dislocation motion law belonging to the class of curvature driven curve dynamics. The work mainly focuses on the simulation of the cross-slip of two dislocation curves where each curve evolves in a different slip plane. The goal is to simulate the motion of the dislocations and to determine the conditions under which the cross-slip occurs. The simulation of the dislocation evolution and merging is performed by improved parametric approach and numerical stability is enhanced by the tangential redistribution of the discretization points.

Key words: partial differential equations, finite difference method, dislocation dynamics, cross-slip, annihilation

Contents

1 Introduction

In the field of material science, dislocations are defined as irregularities or errors in crystal structure of the material. The dislocation is a line defect of the crystalline lattice and it can be represented by a curve closed inside the crystal or by a curve ending on the crystal surface. At low homologous temperatures the dislocations can move only along crystallographic planes (gliding planes) with the highest density of atoms. The motion results in mutual slipping of neighboring parts of the crystal along the gliding planes.

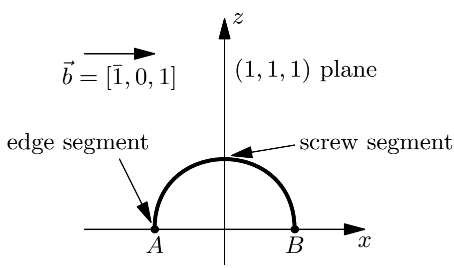

Figure 1: Dislocation types in face-centered cubic metals.

Dislocations are defined by the Burgers vector $\vec{b}$ and the dislocation line. When the Burgers vector is perpendicular to the dislocation line, we say that the dislocation is of an edge type. In case of a screw dislocation, the Burgers vector and dislocation line are parallel. Otherwise, the dislocation is mixed (see Fig. 1). In face-centered cubic metals (fcc), such as copper, silver, and nickel, glide planes are usually crystalographic planes with highest density of atoms (denoted as $(1, 1, 1)$ by Miller indices).

The presence of dislocations strongly influences many of material properties. Also the plastic deformation in crystalline solids is carried by dislocations. Therefore, there is a strong interest in understanding and modeling their behavior without performing expensive experiments. The dislocation research began in 1930s and since that time it became an important branch of material physics. There are numerous theoretical and experimental results. However, complex mathematical models handling dislocation annihilation and cross-slip are still in development. There are atomistic models treating dislocations at the scale of individual atoms or mesoscale models working at the scale of hundreds of nanometers.

However, the dislocation motion may become more complex. Dislocations can undergo the *cross-slip* mechanism. It allows the screw dislocations to change the slip planes and thus to bypass obstacles or to glide to annihilation with a screw dislocation of opposite sign on a neighboring slip plane.Despite of an extended research in the field of cross-slip since 1950s, the cross-slip remains one of the lesser understood aspects of plastic deformation; number of questions related to cross-slip is still open. According to Essman's model of slip irreversibility [10] supported by Weidner and Sauzay measurements [53] the critical annihilation distance is one of the main microstructural parameters. The mechanism controlling the value of this parameter is not yet well known and is the subject of ongoing intense research.

The influence of dislocations and particularly the cross-slip phenomenon justifies the importance of developing suitable mathematical models [24–26, 31, 33, 34, 43, 44] treating the problem. Section 2 deals with the physical background of the proposed dislocation dynamics model, i.e., the motion law, interaction and applied forces, and the channel walls and focuses on its mathematical description. From the mathematical point of view, the dislocations are defined as smooth closed or open planar curves which evolve in time. Their motion is two-dimensional in most cases. The evolving curves can be mathematically described in several ways. One possibility is to use the *level-set method* [11,30,46], where the curve is defined by the zero level of some surface function. One can also use the *phase-field method* [2]. Finally, it is possible to use the *direct (parametric) method* [8,23] where the curve is parametrized in the usual way. The model presented in this work is based on the generalized parametric approach which is able to evolve multiple curves simultaneously. Moreover, the parametric approach does not handle topological changes, therefore, the model contains additional algorithm [34] treating the dislocation merging and splitting.

Section 3 deals with the numerical solution which is obtained by semi-implicit and semi-discrete solver based on finite differences method (FDM) and flowing finite volumes method (FVM) with tangential redistribution [48]. Schemes were verified by comparison with analytical solution and also with other results known from the literature. Simulations of the dislocation dynamics phenomena were done by the finite volume method.

Main results are summed in Section 4. Single dislocation problems, such as the dislocation cycling and the Frank-Read source, serve mainly for the qualitative verification (shapes of dislocations) of the model, while the dislocation bowing simulation provides critical bowing stress values that can be compared with analytical results. The simulation of the dislocation-precipitate interaction, i.e., the formation of Orowan loops and islands (dislocation loops surrounding precipitates or their clusters), is a direct application of the algorithm for topological changes of the dislocations curves. Main focus is paid to the interaction of two dislocations moving towards each other on nearby planes in the PSB channel. Simulations provide passing and cross-slip stresses for various metals and temperatures. Using Brown's criterion [7] the critical cross-slip parameters (critical stress and critical slip plane distance) are obtained.

2 Mathematical model

In the following sections, general dislocation theory described above will be applied to a specific case of one or two gliding dislocations in a channel. The dislocation motion has to take into account all forces acting on the dislocation and in the same time also the dislocation line tension which depends on the curvature. In our case, there are four kind of external forces, i.e., force from the channel walls, interaction force from other dislocations, force caused by the shear stress applied on the crystal, and the friction force of the lattice.

2.1 Dislocation motion law

Dislocations can move in the glide planes mainly by means of applied shear stress and their mutual interaction. The basic equation of the motion of a dislocation curve Γ reads as

$$Bv_\Gamma = F_{total}, \tag{1}$$

where B is the drag coefficient, v_Γ is the velocity of the dislocation motion, and the term F_{total} denotes the sum of all forces per unit length acting on the dislocation curve Γ (including the self-force caused by the dislocation line tension T). Kratochvíl and Sedláček [17] proved that the dislocation self-force can be approximated by the curvature of a corresponding dislocation curve. The self-force term $F_{self} = b\tau_{self}$ where τ_{self} is the stress generated by the dislocation itself can be approximated as $b\tau_{self} = \kappa T$. Thus, the dislocation motion law reads as

$$Bv_\Gamma = T\kappa_\Gamma + F, \tag{2}$$

where $F = F_{app} + F_{int} + F_{wall} - F_{fr}$ is the sum of all forces except dislocation self-force acting on the dislocation:

- $F_{app} = b\tau_{app}$ caused by the resolved shear stress τ_{app} applied on the crystal,
- $F_{int} = b\tau_{int}$ caused by the interaction stress τ_{int} between dislocations in the channel,
- $F_{wall} = b\tau_{wall}$ caused by the stress from channel walls τ_{wall},
- friction $F_{fr} = b\tau_{fr}$ caused by lattice resistance which slows down the movement of the dislocation and must be surpassed in order to move the dislocation. The friction is constant during the simulation.

2.2 Force by channel walls

Dislocations in the persistent slip band channel[1] interact with the dipolar loops clustered in the channel walls, however, it is only a short range interaction. This interaction can be approximately simulated as elastic fields of infinite edge dipoles located in the channel walls. The walls are, in fact, potential valleys generated by the dipoles.

The resolved shear stress in the glide plane produced by an edge dipole consisting of dislocations D_1 and D_2 is obtained by the superposition of their stress fields σ_{xy}

$$\tau_w^{(1)} = \sigma_{xy}^{D_1} - \sigma_{xy}^{D_2} = \frac{Gb}{2\pi}\frac{1}{1-\nu}\left(\frac{x_1(x_1^2-y_1^2)}{(x_1^2+y_1^2)^2} - \frac{x_2(x_2^2-y_2^2)}{(x_2^2+y_2^2)^2}\right), \tag{3}$$

where x_1 and y_1 are the coordinates of a certain point in a channel relative to the edge dislocation D_1. Similarly x_2 and y_2 are coordinates of the same point but relative to edge dislocation D_2. The term G is the shear modulus, ν is the Poisson's ratio and b is the magnitude of the Burgers vector. The interaction with the walls is considered only in the direction of x-axis due to the symmetry of the channel. Similarly, we can derive $\tau_w^{(2)}$ for the other channel wall. The formula for the total resolved shear stress produced by both walls reads as

$$\tau_{wall} = \tau_w^{(1)} + \tau_w^{(2)}. \tag{4}$$

In case of two parallel glide planes, channel walls are considered in the same manner. Each glide plane has its dipoles producing left and right wall. Influences from dipoles related to other planes are not considered.

2.3 Applied force

In face centered cubic metals, the most favorable slip planes are of the $\{1,1,1\}$ type since the atoms are close-packed in these planes. For the our model, we consider, for example, the primary slip system $P : [\bar{1},0,1](1,1,1)$ and its cross-slip system $C :$ $[\bar{1},0,1](1,\bar{1},1)$, see Fig. 2. The primary slip plane $(1,1,1)$ is colored by blue color and the cross-slip plane has a red color. The Burgers vector $\vec{b} = [\bar{1},0,1]$ is common for both planes and in the unit form it reads as $\vec{b}' = [-1/\sqrt{2},0,1/\sqrt{2}]$. Unit normal vector of the primary plane is $n_p = [1,1,1]/\sqrt{3}$ and the cross-slip plane $n_{cs} = [1,-1,1]/\sqrt{3}$. The slip planes form an angle of $\delta = \arccos(1/3) \approx 70.6°$, since

$$\cos\delta = \frac{[1,1,1]\cdot[1,-1,1]}{\sqrt{3}\sqrt{3}} = \frac{1}{3}.$$

If the tensile stress σ_{app} is applied on the crystal in a certain direction, values of the shear stress component in the primary and the cross-slip plane are derived using the Schmid factor (5). The stress in primary plane is given as

$$\tau_p = \sigma_{app}\cos\xi\cos\phi_p, \tag{5}$$

[1]Persistent slip bands (PSB) are lamellae consisting of edge dislocation dipoles usually parallel to the active slip plane with a periodic inner structure of high dislocation density walls and low density of channels

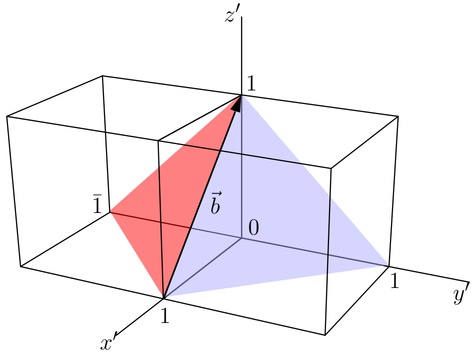

Figure 2: Configuration of the slip planes. Primary plane $(1, 1, 1)$ (blue), cross-slip plane $(1, \bar{1}, 1)$ (red). Burgers vector $\vec{b} = [\bar{1}, 0, 1]$ common for both slip planes.

where ξ is the angle between tensile stress direction and slip direction (the Burgers vector $\vec{b}$) and ϕ_p is the angle between tensile stress direction and Primary plane normal. Similarly, the stress in cross-slip plane is given as

$$\tau_{cs} = \sigma_{app} \cos\xi \cos\phi_{cs}, \tag{6}$$

where ϕ_{cs} is the angle between the tensile stress axis and the cross-slip plane normal.

After some technical work [32], stress values can be derived and read as follows:

$$\tau_{cs} = \frac{1}{3}\sigma_{app} \cos\xi \left(\cos\phi_p \pm 2\sqrt{-\cos(2\xi) - \cos(2\phi_p)}\right), \tag{7}$$

In case of tensile axis lying in the plane defined by the Burgers vector and a normal to the primary plane, i.e., substituting $\phi_p = \pi/2 - \xi$, we get

$$\tau_{cs} = \frac{1}{6}\sigma_{app} \sin(2\xi). \tag{8}$$

Under these conditions the value of the stress in the primary plane is

$$\tau_p = \sigma_{app} \cos\xi \cos\phi_p = \sigma_{app} \cos\xi \cos(\frac{\pi}{2} - \xi) = \frac{1}{2}\sigma_{app} \sin(2\xi). \tag{9}$$

One can see that the stress in the cross-slip plane is 1/3 of the primary plane stress. To maximize both stresses, we chose $\xi = \pi/4$ which yields

$$\tau_p = \frac{1}{2}\sigma_{app}, \qquad \tau_{cs} = \frac{1}{6}\sigma_{app}. \tag{10}$$

2.4 Interaction force

The dislocation motion is influenced not only by external forces applied on the material but also by the interaction force with other dislocations. In our case, dislocations are

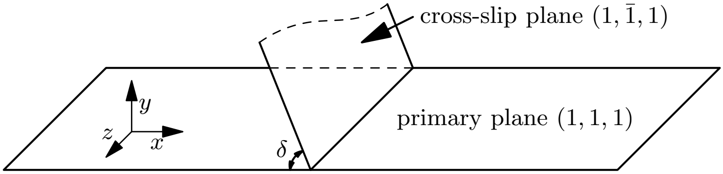

Figure 3: Coordinate transformation. The primary $(1,1,1)$ plane now coincide with xz-plane.

approximated by polygonal curves and all interactions are sums of contributions of straight dislocation segments. In continuous case, sums are substituted by integrals. This section deals with the derivation of the interaction force between dislocations.

The coordinate system x', y', z' of a real crystal introduced in the previous section is rather complicated for the derivation of the model and for the numerical computations. Therefore, the system x', y', z' will be rotated in order to simplify the problem. The new coordinate system x, y, z is shown in Fig. 3. Now the primary plane lies in the xz-plane and the Burgers vector which is parallel with the x-axis reads as $\vec{b} = [b, 0, 0]$ where b is its magnitude.

To determine a stress tensor

$$\sigma_{int}(\vec{x}) = \begin{pmatrix} \sigma_{11} & \sigma_{12} & \sigma_{13} \\ \sigma_{12} & \sigma_{22} & \sigma_{23} \\ \sigma_{13} & \sigma_{23} & \sigma_{44} \end{pmatrix}, \qquad (11)$$

in the x, y, z coordinate system at a location $\vec{x}$ from a straight dislocation segment AB (see Fig. 4), we use Devincre's formula for three dimensional stress field [9]. The formula provides a stress tensor from a dislocation half-line from A to infinity in the direction of $\vec{w}$ and reads as

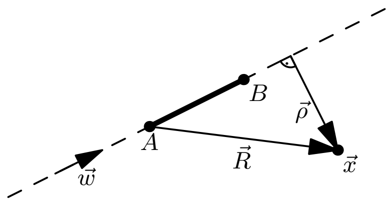

Figure 4: Stress field from the dislocation segment AB at a location $\vec{x}$ and corresponding vectors.

$$\sigma_{ij}^A = \frac{G}{4\pi}\frac{1}{R(U+R)}\Bigg[(\vec{b}\times\vec{Y})_i w_j + (\vec{b}\times\vec{Y})_j w_i - \frac{1}{1-\nu}\big((\vec{b}\times\vec{w})_i Y_j + (\vec{b}\times\vec{w})_j Y_i\big) - \frac{(\vec{b},\vec{\rho},\vec{w})}{1-\nu}\Big[\delta_{ij} + w_i w_j + \frac{(\rho_i w_j + \rho_j w_i + U w_i w_j)(U+R)}{R^2} + \frac{\rho_i\rho_j(2+U/R)}{R(U+R)}\Big]\Bigg],$$

where the meaning of terms is as follows:

$\vec{w}$	tangential vector of the dislocation segment,
$\vec{R}$	vector to the location $\vec{x}$ from A,
R	$= \sqrt{R_1^2 + R_2^2 + R_3^2}$,
U	$= \vec{R} \cdot \vec{w}$,
Y_i	$= R_i + \vec{R} w_i$,
$\vec{\rho}$	$= \vec{R} - U\vec{w}$ normal component of $\vec{R}$ to the dislocation segment,
$\vec{b}$	Burgers vector of the dislocation,
G	shear modulus,
i, j	$= 1,2,3$, (x-axis, y-axis, z-axis)
ν	Poisson's ratio,
δ_{ij}	Kronecker symbol,
$(\vec{b}, \vec{\rho}, \vec{w})$	is the triple product $(\vec{b}, \vec{\rho}, \vec{w}) = \vec{b}(\vec{\rho} \times \vec{w})$.

The stress tensor generated by a straight finite dislocation segment AB is then given as

$$\sigma_{int}(\vec{x}) = \sigma_{ij} = \sigma_{ij}^A(\vec{x}) - \sigma_{ij}^B(\vec{x}). \tag{12}$$

The stress field causes forces that act on the dislocation at position $\vec{x}$. We use Peach-Koehler formula [45] to compute forces on the dislocation exposed to a stress field σ_{int} generated by other dislocations. The formula reads as

$$\vec{F}_{int} = (\sigma_{int}\vec{b}) \times \vec{w}, \tag{13}$$

where $\vec{b}$ is the Burgers vector of the dislocation and $\vec{w}$ is its tangential vector. Note that $\vec{F}_{int}$ is always perpendicular to the plane defined by $\vec{b}$ and $\sigma_{int}\vec{b}$, and is always perpendicular to $\vec{w}$. The motion is caused by the normal component of $\vec{F}_{int}$ to the dislocation in the slip plane. The projection is done simply by a dot product with the normal vector to the dislocation $\vec{n}$ in the slip plane, i.e.,

$$F_{int} = \vec{F}_{int}\vec{n}. \tag{14}$$

The Burgers vector $\vec{b} = (b, 0, 0)$ is parallel with the x-axis and the primary slip plane parallel with the xz-plane. Hence, the unit tangential vector of the dislocation has the form $\vec{w}_p = (w_1, 0, w_3)$ and the unit normal vector $\vec{n}_p = (w_3, 0, -w_1)$. Vectorial force is given by

$$\vec{F}_{int}^{(p)} = (\sigma_{int}\vec{b}) \times \vec{w}_p = b \begin{pmatrix} \sigma_{11} \\ \sigma_{12} \\ \sigma_{13} \end{pmatrix} \times \vec{w}_p = b(\sigma_{12}w_3, \sigma_{13}w_1 - \sigma_{11}w_3, -\sigma_{12}w_1),$$

and the normal component in the xz-plane

$$F_{int}^{(p)} = \vec{F}_{int}^{(p)}\vec{n}_p = b(\sigma_{12}w_3^2 + \sigma_{12}w_1^2) = b\sigma_{12}(w_3^2 + w_1^2) = b\sigma_{12}. \tag{15}$$

Similarly, we can derive the force in the cross-slip plane having angle δ with the xz-plane. The tangential vector of the dislocation is defined as $\vec{w}_{cs} = (w_1, w_3 \tan\delta, w_3)$ and the normal vector in the cross-slip plane $\vec{n}_{cs} = (w_3(\tan^2\delta + 1), -w_1 \tan\delta, -w_1)$. Vectorial force is given by

$$\vec{F}_{int}^{(cs)} = (\sigma_{int}\vec{b}) \times \vec{w}_{cs} = b(\sigma_{12}w_3 - \sigma_{13}w_3 \tan\delta, \sigma_{13}w_1 - \sigma_{11}w_3, \sigma_{11}w_3 \tan\delta - \sigma_{12}w_1),$$

and the normal component in the cross-slip plane

$$
\begin{aligned}
F_{int}^{(cs)} &= \vec{F}_{int}^{(cs)} \vec{n}_{cs} = \qquad (16) \\
&b\sigma_{12}(w_3^2 \tan^2 \delta + w_3^2 + w_1^2) \\
&+ b\sigma_{11}(w_1 w_3 \tan \delta - w_1 w_3 \tan \delta) \\
&+ b\sigma_{13}(-w_3^2 \tan^3 \delta - w_3^2 \tan^2 \delta - w_1^2 \tan \delta) \\
&= b\sigma_{12} - b\sigma_{13} \tan \delta. \qquad (17)
\end{aligned}
$$

One can easily see that for $\delta = 0$, i.e., for the primary plane, (17) provides the same result as (15).

The stress field generated by a polygonal dislocation curve is a sum of stresses of all segments. Let us consider a polygonal dislocation curve $Y = \{Y_1, \cdots, Y_N\}$. Then the total stress from the dislocation Y at point X is given by

$$
\sigma_{ij}^{Y}(X) = \sum_{k=1}^{N-1} \sigma_{ij}^{Y_k}(Z_i) - \sigma_{ij}^{Y_{k+1}}(Z_i). \qquad (18)
$$

In case of two interacting dislocations $Y = \{Y_1, \cdots, Y_N\}$ and $Z = \{Z_1, \cdots, Z_M\}$, one has to compute stress field from one dislocation at every point of the second dislocation. see Fig. 5.

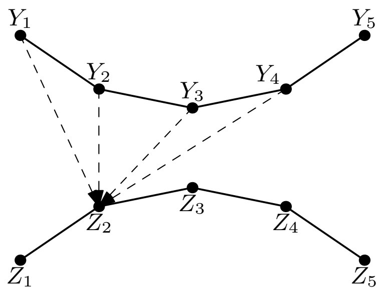

Figure 5: Tension from dislocation Y on Z by (19).

$$
\sigma_{ij}(Z_i) = \sum_{k=1}^{N-1} \sigma_{ij}^{Y_k}(Z_i) - \sigma_{ij}^{Y_{k+1}}(Z_i), i, j \in 1, 2, 3. \qquad (19)
$$

2.5 Cross-slip criterion

The model treats several dislocation phenomena, including the cross-slip mechanism where dislocations can change slip planes if another one is favorable. To formulate the cross-slip criterion, i.e., to specify the cross-slip conditions, we consider two dislocations of opposite sign in two parallel primary slip planes η_1 and η_2 (see Fig. 6). The dislocations in a channel of persistent slip bands are initially kept apart in straight screw positions. As the dislocations are pushed by the applied stress between two channel walls in the opposite directions, they bow out and attract each other. One of three scenarios may occur:

a) reaching the cross-slip geometry (see Fig. 6), the screw tips of the dislocations are forced to enter the cross-slip plane. There the dislocation segments spread and their screw parts annihilate,

b) the dislocations remain in the primary slip planes and form a dipole,

c) the dislocations in the primary slip planes separate and escape each other.

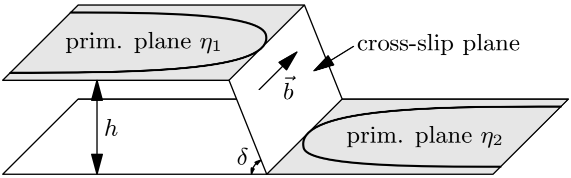

Figure 6: Dislocations at the cross-slip configuration when the cross-slip criterion is evaluated.

Our objective is to determine the distance between the primary slip planes critical for the cross-slip annihilation and to simultaneously estimate the saturation stress needed for the escape. For this purpose *Brown's criterion* [7] is used: *the saturation stress in cycling is controlled by the stress required to separate two screw dislocations of opposite sign, which are just on the point of mutual annihilation by cross-slip.*

Let us consider that the tips of the dislocations are reaching the cross-slip configuration shown in Fig. 6. We compare the force $b\tau_p$ pushing the tips into the primary planes and the force $b\tau_{cs}$ pushing them into the cross-slip plane at the moment when the screw tips touch the intersection lines of the primary planes and the cross-slip plane. At this "cross-road" where the dislocations are still in the primary slip planes the friction stress τ_{fr}, the curvature κ and the stress exerted by walls τ_{wall} are the same for both directions. The applied stress and the interaction stress resolved into either the primary planes or the cross-slip plane are the only quantities which differ. The forces $b\tau_p$ and $b\tau_{cs}$ are given as follows:

$$
\begin{aligned}
b\tau_p &= T\kappa + b(\tau_{int}^{(p)} + \tau_{wall} + \tau_{app} - \tau_{fr}),\\
b\tau_{cs} &= T\kappa + b(\tau_{int}^{(cs)} + \tau_{wall} + \tau_{app}/3 - \tau_{fr}),
\end{aligned}
$$

where $\tau_{int}^{(p)}$ represents the interaction stress provided the dislocations are going to continue the motion in the primary planes, $\tau_{int}^{(cs)}$ is the interaction stress provided the dislocations enter the cross-slip plane, τ_{app} is the resolved shear stress component of the applied stress in the primary planes. In the evaluation of the resolved shear stress component $\tau_{app}/3$ in the cross-slip plane we assume that the angle between the loading axis and the normal to the primary slip planes is $\pi/4$, i.e. the orientation of the loading axis is in the center of the standard stereographic triangle. The derivation is provided in Section 2.3. Let us note that for modeling the whole cross-slip annihilation process the curvature in the cross-slip plane has to be defined and calculated. In [38] where the annihilation process and overcoming obstacles by cross-slip are modeled it is demonstrated that the curvature smoothly continues in the cross-slip plane and that the difference in the curvatures in the cross-slip plane and in the primary planes just after the "cross-road" is about 3% (see the last paragraph in Section 2.6). The cross-slip criterion is then formulated as follows:

- cross-slip occurs, whenever $\tau_{cs} > \tau_p$,
- primary slip continues, whenever $\tau_{cs} \leq \tau_p$.

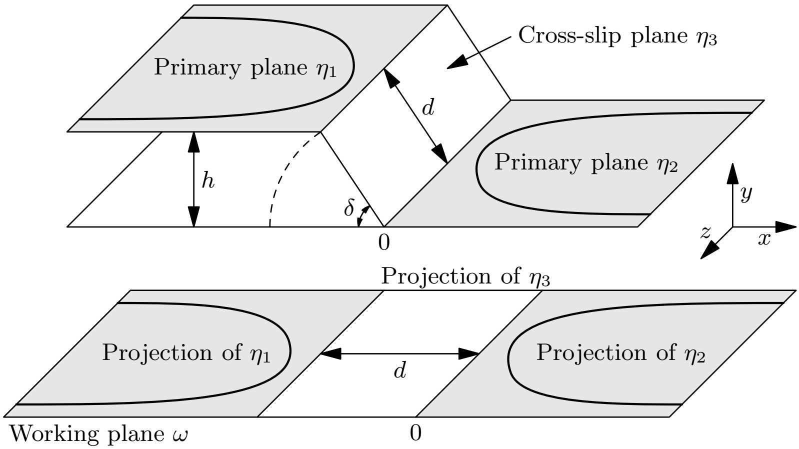

Figure 7: Mapping between two and three dimensional model. Forces on dislocations are evaluated in 3D in planes η_1, η_2, η_3 and then projected into 2D to the working plane ω for the computation by mean curvature flow equation (2). The mapping works similarly to “folding a box”.

2.6 Model for dislocations in non-parallel planes

The phenomenon of cross-slip is related to the interaction between the dislocations in different slip planes and to the topological change in dislocation configuration leading to the connection of different slip planes through the cross-slip plane transversal to the slip planes.

The model of cross-slip is based on evolution law (2), treated in slip planes, evaluating the force interaction between the dislocations by means of the Devincre’s formula (see Section 2.4) and following the criterion of cross-slip and dislocation topological change. As far as the cross-slip plane is transversal to the slip planes, the model explores the three-dimensional nature of the force interaction. The motion laws for dislocation curves $\Gamma_{\eta_1}, \Gamma_{\eta_2}, \Gamma_{\eta_3}$ in slip planes η_1 and η_2 and the cross-slip plane η_3 are given by

$$Bv_i = T\kappa_i + F_i(\vec{X}, t), \quad i \in \{\eta_1, \eta_2, \eta_3\}, \tag{20}$$

where again B is the drag coefficient, T is the line tension, and v_i and κ_i are normal velocity and curvature of the dislocation under the force F_i in their respective planes η_1, η_2, η_3, i.e.,

$$F_{\eta_{1,2}} = \begin{cases} F_{wall}(\vec{X}, t) + F_{app}^{(p)} + F_{int}^{(p)} - F_{fr} & \text{if } F_{wall}(\vec{X}, t) + F_{app}^{(p)} + F_{int}^{(p)} > F_{fr} \\ 0 & \text{otherwise;} \end{cases}$$

$$F_{\eta_3} = \begin{cases} F_{wall}(\vec{X}, t) + F_{app}^{(cs)} + F_{int}^{(cs)} - F_{fr} & \text{if } F_{wall}(\vec{X}, t) + F_{app}^{(cs)} + F_{int}^{(cs)} > F_{fr} \\ 0 & \text{otherwise.} \end{cases}$$

Under the conditions considered in Section 2.3 the forcing terms read as

$$F_{app}^{(cs)} = \frac{1}{3} F_{app}^{(p)}, \qquad F_{int}^{(p)} = b\sigma_{12}, \qquad F_{int}^{(cs)} = b\sigma_{12} - b\sigma_{13} \tan\delta.$$

Mathematical treatment of this model is based on the projection of dislocation motion laws in different planes into one working plane ω. This projection preserves shape of the dislocation curves and forces acting on them in the normal direction.

The three-dimensional real configuration of the physical model is shown in the upper part of Figure 7 and the configuration projected to ω in the lower part of Figure 7.

The dislocations are contained in the parallel primary slip planes η_1 and η_2 the distance h apart. The cross-slip plane with angle δ against the primary plane η_2. Then, the length d of the cross-slip plane segment between η_1 and η_2 is $d = h/\sin\delta$.

The projection Φ into the working plane ω is described as follows:

Denote the coordinates related to the plane η_1 as $(x_{\eta_1}, y_{\eta_1}, z_{\eta_1})$, to the plane η_2 as $(x_{\eta_2}, y_{\eta_2}, z_{\eta_2})$, to the plane η_3 as $(x_{\eta_3}, y_{\eta_3}, z_{\eta_3})$, and to the plane ω as $(x_\omega, y_\omega, z_\omega)$. Assume that the intersection $\eta_1 \cap \eta_3$ corresponds to the line $x_{\eta_1} = -d\cos\delta = -h\cot\delta$ and the intersection $\eta_2 \cap \eta_3$ corresponds to the line $x_{\eta_2} = 0$.

Then the mapping Φ from $\eta_1 \cup \eta_2 \cup \eta_3$ to ω is given as follows:

$$\vec{X}_\omega = (x_\omega, y_\omega, z_\omega) = \begin{cases} (x_{\eta_1} - d(1-\cos\delta), 0, z_{\eta_1}) & \text{for } \vec{X}_{\eta_1} \in \eta_1, \\ (x_{\eta_2}, 0, z_{\eta_2}) & \text{for } \vec{X}_{\eta_2} \in \eta_2, \\ (x_{\eta_3}/\cos\delta, 0, z_{\eta_3}) & \text{for } \vec{X}_{\eta_3} \in \eta_3. \end{cases} \tag{21}$$

The inverse mapping Φ^{-1} from ω to $\eta_1 \cup \eta_2 \cup \eta_3$ is given by

$$\begin{array}{lll} \vec{X}_{\eta_1} & = (x_{\eta_1}, y_{\eta_1}, z_{\eta_1}) = (x_\omega + d(1-\cos\delta), 0, z_\omega) & \text{for } x_\omega < -d, \\ \vec{X}_{\eta_2} & = (x_{\eta_2}, y_{\eta_2}, z_{\eta_2}) = (x_\omega, 0, z_\omega) & \text{for } x_\omega > 0, \\ \vec{X}_{\eta_3} & = (x_{\eta_3}, y_{\eta_3}, z_{\eta_3}) = (x_\omega \cos\delta), -x_\omega \sin\delta, z_\omega) & \text{for } x_\omega \in \langle -d, 0 \rangle, \end{array} \tag{22}$$

At first, the forces on dislocations are computed and then the geometry is projected into the working plane ω. After the projection, the curve motion is treated as a multiple dislocation problem including topological changes described later. When the equation of motion is applied, the working plane ω is mapped back to planes η_1, η_2, and η_3.

3 Numerical approximation

The equation of motion (2) is treated by the parametric (direct) approach. In this case, the planar curve $\Gamma(t)$ is described by a smooth time-dependent vector function

$$\vec{X} : I_u \times I_t \to \mathbb{R}^2,$$

where $I_t = [0, t_{max}]$ is the time interval and $I_u = [0, 1]$ is a fixed interval for the curve parameter. For open curves we consider usual closed unit interval, while for closed curves a circle of length 1 is taken to ensure curve smoothness on the interval boundary. The curve $\Gamma(t)$ is then given as the set

$$\Gamma(t) = \{\vec{X}(u,t) = ({}^1X(u,t), {}^2X(u,t)), u \in I_u\},$$

where ${}^1X(u,t)$, ${}^2X(u,t)$ are the components of $\vec{X}(u,t)$. The family of curves satisfies the equation of motion (2).

The unit tangential vector $\vec{w}$ is defined as $\vec{w} = \partial_u \vec{X}/|\partial_u \vec{X}|$. The unit normal vector $\vec{n}$ is perpendicular to the tangential vector and $\vec{n}\vec{w} = 0$ holds, i.e., $\vec{n} = \partial_u \vec{X}^{\perp}/|\partial_u \vec{X}|$ where $\vec{X}^{\perp}$ is a vector perpendicular to $\vec{X}$. In case of closed curve, $\vec{n}$ is the inner vector to the interior of the curve. In case of open curve, $\vec{n}$ has a selected, pre-defined direction (e.g., upwards). The orientation of the curve is clockwise.

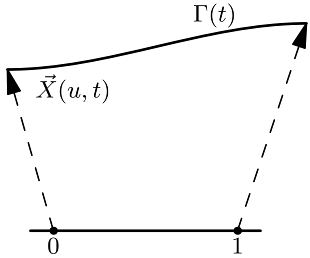

Figure 8: Parametric method. The curve is mapped from a fixed interval $[0, 1]$.

Using the Frenet formulae (see e.g. [47]), one can determine the curvature

$$\kappa_\Gamma = \frac{\partial_{uu}\vec{X}}{|\partial_u \vec{X}|^2} \cdot \frac{\partial_u \vec{X}^{\perp}}{|\partial_u \vec{X}|} = \vec{N} \cdot \frac{\partial_{uu}\vec{X}}{|\partial_u \vec{X}|^2}.$$

The normal velocity v_Γ is defined as the time derivative of $\vec{X}$ projected into the normal direction,

$$v_\Gamma = \partial_t \vec{X} \cdot \frac{\partial_u \vec{X}^{\perp}}{|\partial_u \vec{X}|}.$$

To improve numerical stability of the computation, tangential term α is added to the equation[2]. Tangential motion of the discretization points is called *redistribution of the discretization points*. Subtituting above quantities and multiplying by $\vec{n}$, we obtain the differential equation for the curve motion as follows

$$B\partial_t \vec{X} = T\frac{\partial_{uu}\vec{X}}{|\partial_u \vec{X}|^2} + \alpha\frac{\partial_u \vec{X}}{|\partial_u \vec{X}|} + F(\vec{X}, t)\frac{\partial_u \vec{X}^{\perp}}{|\partial_u \vec{X}|}. \tag{23}$$

This equation is accompanied either by the periodic boundary conditions

$$\vec{X}(0,t) = \vec{X}(1,t),$$

for closed dislocation curves, or with fixed ends boundary conditions

$$\vec{X}(0,t) = \vec{X}_{\text{fixed},0}, \ \vec{X}(1,t) = \vec{X}_{\text{fixed},1},$$

for open dislocation curves. The initial condition for the curve position is prescribed as

$$\vec{X}(u,0) = \vec{X}_{\text{ini}}(u).$$

The term α is described in detail in [48–50].

[2] When tracking a curve motion, usually only terms in normal direction to the curve are taken into account since tangential terms do not affect the shape of the curve (for more details, see [12, Proposition 2.4]).

3.1 Topological changes algorithm

The algorithm we present is not supposed to be universal for every situation and possibility. Main purpose is to simulate topological changes that can occur during dislocation dynamics, i.e., topological changes such as annihilation (merging) of dislocation curves, multiplication of curves on encounter, etc. As the initial condition, we consider only curves which do not intersect itself and do not touch each other. The orientation of curves is clockwise. The algorithm is designed for topological changes of curves which touch only at one point. More complex changes can be treated by multiple application of the algorithm in one time step. The evolution after merging or splitting behaves as expected. Normal vectors and evolution speed correspond to the situation captured by the level-set method. The results of the algorithm are compared with the level-set method later in this chapter.

Let us consider two closed or open curves Γ_1 and Γ_2 discretized as $X = \{x_1, x_2, \cdots, x_n\}$ and $Y = \{y_1, y_2, \cdots, y_m\}$ in $\mathbb{R}^2$. The curves evolve independently according to the equation (23). The algorithm for merging two curves is as follows:

1. Compute the distance between X and Y and find one point from each curve where the minimum is reached. Let us denote the distance as d, the point from X as x_{min} and from Y as y_{min}.
2. Check if the distance d between curves is smaller than a given tolerance ϵ. If not, compute new time-step and go to 1.
3. Create a new curve Z. We must take into account the type of merged curves. Merging two closed curves will produce one closed curve. Merging one open and one closed curve will produce one open curve and merging two open curves will produce two open curves.
4. Copy points from X from the beginning (i.e., from x_1) up to x_{min} to Z. Figure 9a; segment A (green).
5. Copy points from Y from y_{min} up to the end (i.e., up to y_m) to Z. Figure 9a; segment B (blue).
6. Copy points from Y from the beginning (i.e., from y_1) up to y_{min} to Z. Figure 9a; segment C (brown).
7. Copy points from X from x_{min} up to the end (i.e., up to x_n) to Z. Figure 9a; segment D (black).
8. Delete X and Y.
9. Compute a new time-step for Z and go to 1.

Note that in case of two open curves, it is necessary to create two new curves Z_1 and Z_2 and copy the points there.

We also consider that one curve can touch itself and thus split itself into 2 parts. Let us consider a closed or open curve discretized as $X = \{x_1, x_2, \cdots, x_n\}$. The curve evolves independently according to the equation (23). The algorithm for splitting into two curves is as follows:

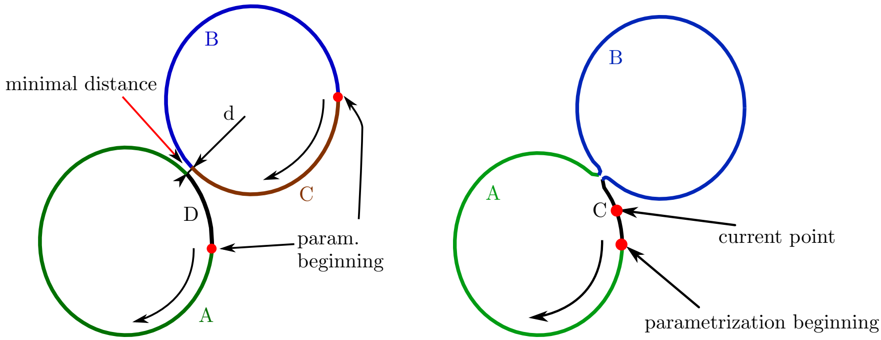

(a) Merging of two curves. (b) Splitting of one curve.

Figure 9: Algorithm for topological changes.

1. Compute the distance between points in X and find two points where the minimum was reached. Let us denote the distance as d, and the points as x_{min1} and x_{min2}. We do not consider several points in the neighborhood of each point when measuring the distance to avoid finding minimal distance for two neighboring points. The number has to be computed according to the value of a given tolerance ϵ (see the next step). We recommend to omit all points with the distance smaller than at least 4ϵ. In Figure 9b, the algorithm for the distance computation starts several discretization points after the current point and ends several points before the current active point.

2. Check if the distance d between points is smaller than a given tolerance ϵ. If not, compute new time-step and go to 1.

3. Create two new empty curves Y and Z. If X is an open curve, Y will be open and Z closed curve. If X is a closed curve then Y and Z will be closed curves.

4. Copy points from X from the beginning (i.e., from x_1) up to x_{min1} to Y. Figure 9b; segment A (green).

5. Copy points from X from x_{min1} up to x_{min2} to Z. Figure 9b; segment B (blue).

6. Copy points from X from x_{min2} up to the end (i.e., up to x_n) to Y. Figure 9b; segment C (black).

7. Delete X.

8. Compute new time-step for Y and Z and go to 1.

The most important parameter for presented algorithm and also its biggest drawback is the threshold parameter ϵ. Its correct value depends on the number of discretization points and on the speed of curve evolution. For the algorithm to work correctly, it must be higher than the maximal length of curve segments and also higher than distance between two following time levels. Too small value may cause the algorithm to miss the touching point of the curves. Such situation may provide unexpected results, such as crossing of the curves without merging of splitting, or topological changes in wrong parts of the curves. On the other hand, too large value causes premature topological change reducing accuracy of the computation. Therefore, when a higher accuracy of merging or splitting is required, the curve must have a fine spatial discretization (causing higher computation times) and relatively small time-step. Recommended value of ϵ is about

$$\epsilon \approx 2 \max_{i=1,\dots,N} \{|X_i - X_{i-1}|\}. \tag{24}$$

The algorithm works best with a uniform tangential redistribution of points since it keeps the distance between points constant. With curvature adjusted redistribution, the algorithm may fail when ϵ is too small or one has to choose sufficiently large ϵ according to formula above.

3.2 Algorithm of discrete dislocation dynamics

The complete algorithm for the discrete dislocation dynamics of l dislocation curves $X_i, i = 1, \dots, l$ in slip primary slip planes η_1, η_2, and cross-slip plane η_3 (Fig. 7) is given as follows:

1. Set up all constants required for the simulation and generate initial shapes of the dislocation curves $X_i, i = 1, \dots, l$. Curves cannot overlap.
2. Compute reciprocal interaction forces F_{int}^{ij}between dislocations X_i and X_j, $i \neq j$, where $i, j = 1, \dots, l$ using Devincre's formula for polygonal dislocations.
3. Compute forces from channel walls F_{wall}^{i} for dislocation X_i, $i = 1, \dots, l$.
4. Map all dislocations $X_i, i = 1, \dots, l$ into a working plane ω using the mapping Φ (21).
5. Run the algorithm for topological changes for all dislocations $X_i, i = 1, \dots, l$ in working plane ω. Update the value of l if some dislocations merged or split.
6. Compute new time level for $X_i, i = 1, \dots, l$ using the finite volume method with the uniform redistribution of discretization points.
7. Map $X_i, i = 1, \dots, l$ from working plane ω into the three dimensional space of planes η_1, η_2, η_3 using Φ^{-1} (22).
8. If the simulation time is smaller than the given maximal time t_{max}, go to 2, else finish.

There are many possibilities of the algorithm optimization. Most simulations occurred only in primary slip planes, thus, we can omit steps 4 and 7. The interaction computation can be performed in every second or third time-step as explained in the previous section. The uniform redistribution allows us to lower the number of discretization points. We recommend to use approximately 120–150 nodes. If the dislocations cannot touch (i.e., lie on different slip planes), it is recommended to skip the topological changes algorithm.

Metal	Temperature ϑ [K]	Shear mod. G [GPa]	Channel width d_c [nm]	Friction τ_{fr} [MPa]	Energy E [nJ·m^{-1}]
copper	430	40	2140	3	1.97
	295	42	1200	4	2.15
	190	44	1050	5	2.16
	77	45	700	7	2.21
	4.2	46	450	9	2.27
nickel	750	49	6100	1	2.41
	600	53	3000	2	2.61
	293	63	1200	4	3.1
	77	68	600	7	3.35
silver	293	26.2	1200	4	1.73

Table 1: Material constants for copper, nickel and silver at various temperatures.

4 Results

The mathematical model presented in this work allows us to simulate various phenomena involving dislocation dynamics, such as single dislocation problems (dislocation cycling, dislocation bowing from a channel wall, the dislocation glide through the PSB channel) and multiple dislocation problems (interaction of two and more dislocations, dislocation cross-slip, estimation of the passing stress and the interaction with rigid obstacles). We mainly focus on the simulation of double cross-slip with annihilation which is the most important contribution of this work to the problems of dislocation dynamics.

Material constants used for simulations are stated in Table 1. The shear modulus G used for copper simulations is taken from [14, 21] (the values for temperatures 4 K and 430 K have been extrapolated). For nickel the values of G are taken from [52]. The shear modulus G for silver is determined by the anisotropic cubic elastic constants $C_{11} = 122$ GPa, $C_{12} = 91.5$ GPa, $C_{44} = 44.8$ GPa.

$$G_{Ag} = \sqrt{C_{44}\frac{C_{11} - C_{12}}{2}} = 26.2 \text{ MPa}.$$

The channel width d_c is it taken from [1, 13, 14, 28]. The value 1200 nm for the channel width in silver was deduced from the micrograph Fig. 7d in [22]. For τ_{fr} in copper we employed data from [13] for the temperature dependent friction stress in PSB channel (the value at temperature 4 K is extrapolated). The values for the friction stress τ_{fr} in nickel and silver are taken the same as in copper; for higher temperature the values for nickel have been extrapolated. The cross-slip angle $\lambda = 71^\circ$ corresponds to the fcc crystal geometry (see Section 2). The drag coefficient $B = 1.0 \cdot 10^{-5}$ Pa · s is taken the same for copper, nickel and silver.

The edge dislocation energy E for copper, nickel, and silver is computed using

$$E = \frac{1}{1-\nu}\frac{Gb^2}{2}.$$

quantity	copper	nickel	silver
Burgers vector magnitude b [nm]	0.256	0.255	0.288
Poisson's ratio ν	0.34	0.31	0.37

Table 2: Burgers vector and Poisson's ratio for copper, nickel, and silver.

The value of $E^{(e)}$ for copper at $\vartheta = 295$ K is chosen so that the values of the line tension T fit the experimental values $T \approx 0.3$ nN for an edge dislocation and $T \approx 3.3$ nN for a screw dislocation [27]. The line tension T is computed according to

$$T(\zeta) = E\big(1 - \nu\cos^2\zeta + 2\nu\cos 2\zeta\big) = E\big(1 - 2\nu + 3\nu\cos^2\zeta\big).$$

The values for Poisson's ratio ν and the magnitude of the Burgers vector for copper, nickel, and silver are taken according to Table 2.

4.1 Frank-Read source

The Frank-Read source describes a way how dislocations can multiply by generating new dislocation loops (closed curves). The mechanism is dealt in detail in [15, 16, 29]. Experiment 1 and corresponding Figure 10 shows the simulation of the Frank-Read mechanism. The open dislocation curve is fixed at $(-400, 0, 0)$ and $(400, 0, 0)$ and is forced to bow out under the applied shear stress $\tau_{app} = 60$ MPa. In case of low applied stress, the dislocation would stop in a stable position, therefore, some higher value is required. The evolution continues to evolve until the curve touches itself. The position and location of the contact is detected by the algorithm for topological changes. The algorithm computes the distance of the curve points each time step and when the distance drops below the numerical parameter ϵ, the curve splitting is performed. In this particular simulation ϵ is set to 5 nm. The algorithm splits the curve into one open dislocation line with ends fixed at the same positions as the original line dislocation and one dipolar loop (closed curve). The loop continues in expansion and the dislocation line will again undergo the same process. The Frank-Read source cannot generate unlimited number of dislocation loops because new loops interact with each other and slow down the source. This phenomena is not covered by our model.

The tangential redistribution is very important for the simulations involving topological changes. In case of no tangential motion, the algorithm may fail since the distance between discretization points is variable (usually accumulated in some part of the curve). The uniform redistribution, which keeps the relative distance between discretization points constant, is the safest and usually the best choice for the algorithm. However, in this particular case, we can choose also curvature adjusted redistribution and obtain slightly higher precision of the splitting because the expected touching point of the curve is in a part with high curvature. Redistribution values in this experiment (Experiment 1) are $\rho = 100$ and $\varepsilon = 0.1$. The value of ρ is usually chosen higher for the curvature adjusted redistribution than for the uniform redistribution in order to achieve faster redistribution and shorter computational time.

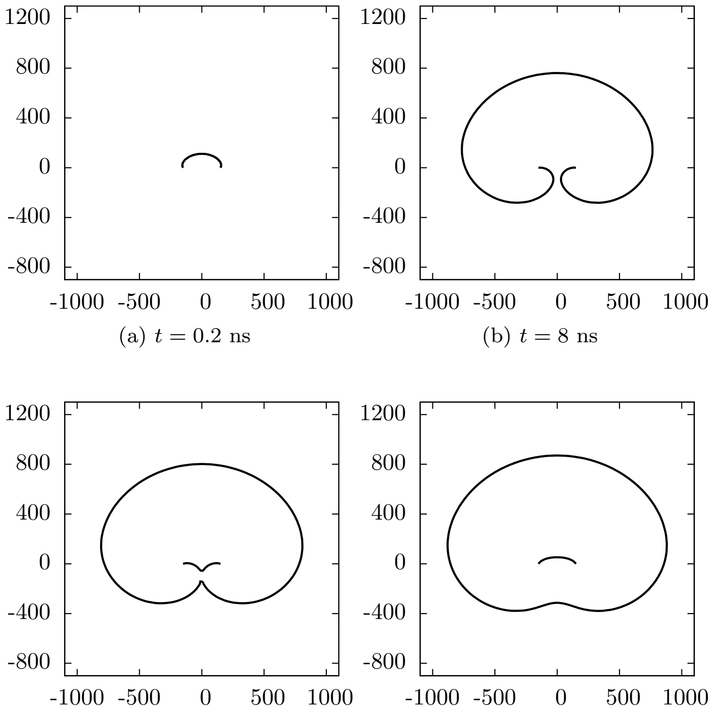

(a) $t = 0.2$ ns (b) $t = 8$ ns

(c) $t = 1.3$ ns (d) $t = 1.46$ ns

Figure 10: Simulation of the Frank-Read source. Experiment 1.

Experiment 1. The Frank-Read mechanism of dislocation multiplication.
Initial condition: Line, $\Gamma_0 = (-400 + 800u, 0, 0)$, $u \in [0, 1]$.
Physical parameters: $B = 10^{-5}$ Pa $\cdot$ s, $b = 0.256$ nm, $\nu = 0.34$, $G = 42.1$ GPa
Numerical parameters: 300 nodes, curvature adjusted redistribution, $\rho = 100$, $\varepsilon = 0.1$.
External stress: $\tau_{app} = 60$ MPa.
Figure: Fig. 10.

4.2 Dislocation-precipitate interaction

Dislocations can interact with other defects through the stress field. If the obstacle stress field is weak, the dislocation may pass through the obstacle without spitting. In case of the strong stress field generated by the obstacle, the dislocation movement is blocked and the dislocation will surround the obstacle.

The experiment 2 and Figure 11 illustrate the combination of all previous phenomena. There is one weak obstacle in the lower left corner, cluster of 7 strong obstacles and one stand-alone obstacle in the top left corner. The dislocation moves under the applied stress $\tau_{app} = 40$ MPa. The dislocation passes through the weak obstacle and then surrounds the cluster of obstacles creating so called *Orowan island*. The stand-alone obstacle causes one *Orowan loop*.

The dislocation (Orowan) loops around obstacles generate a stress field that influences other dislocations. If there is another dislocation passing in the vicinity of surrounded obstacles, some higher applied stress would be necessary. The dislocation motion is more difficult and *material hardening* occurs.

The simulation was performed with the algorithm for topological changes turned on (fixed distance parameter $\epsilon = 3$ nm) and with the uniform tangential redistribution.

Experiment 2. Evolution through a random cluster of obstacles. Obstacle in the lower left corner is a weak precipitate.
Initial condition: $\Gamma_0 = (-600 + 1200u, 0, 0)$, $u \in [0, 1]$.
Physical parameters: $B = 10^{-5}$ Pa $\cdot$ s, $b = 0.256$ nm, $\nu = 0.34$, $G = 42.1$ GPa
Numerical parameters: 300 nodes, uniform redistribution.
External stress: $\tau_{app} = 40$ MPa.
$\tau^{(1)}_{obst} = 150$ MPa, $\vec{x}_{obst} = (200, 0, 800)$ nm, $r_{obst} = 60$ nm;
$\tau^{(2)}_{obst} = 150$ MPa, $\vec{x}_{obst} = (-200, 0, 800)$ nm, $r_{obst} = 60$ nm;
$\tau^{(3)}_{obst} = 150$ MPa, $\vec{x}_{obst} = (0, 0, 800)$ nm, $r_{obst} = 60$ nm;
$\tau^{(4)}_{obst} = 150$ MPa, $\vec{x}_{obst} = (100, 0, 980)$ nm, $r_{obst} = 60$ nm;
$\tau^{(5)}_{obst} = 150$ MPa, $\vec{x}_{obst} = (-100, 0, 960)$ nm, $r_{obst} = 60$ nm;
$\tau^{(6)}_{obst} = 150$ MPa, $\vec{x}_{obst} = (0, 0, 1160)$ nm, $r_{obst} = 60$ nm;
$\tau^{(7)}_{obst} = 150$ MPa, $\vec{x}_{obst} = (-360, 0, 1340)$ nm, $r_{obst} = 60$ nm;
$\tau^{(8)}_{obst} = 150$ MPa, $\vec{x}_{obst} = (-100, 0, 1340)$ nm, $r_{obst} = 60$ nm;
$\tau^{(9)}_{obst} = 50$ MPa, $\vec{x}_{obst} = (-300, 0, 700)$ nm, $r_{obst} = 60$ nm.
Figure: Fig. 11.

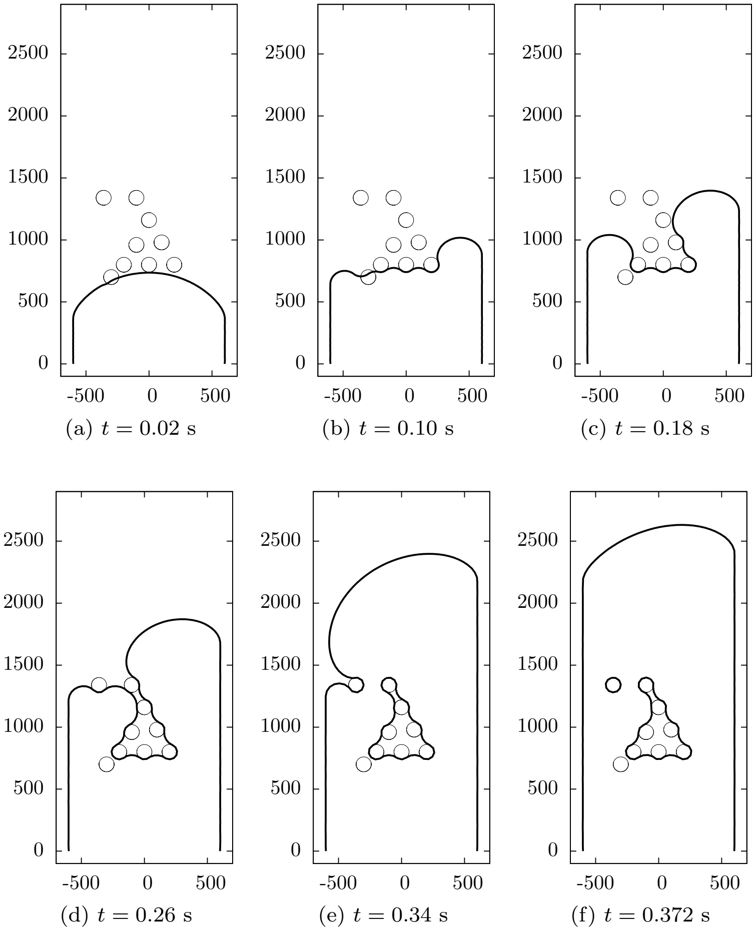

Figure 11: Evolution through a random cluster of obstacles, weak obstacle and Orowan island, $\tau_{app} = 40$ MPa, $t \in (0, 0.26)$, curve discretized by $M = 300$ nodes, dimensions in nm. Experiment 2

4.3 Estimation of critical cross-slip parameters

The estimation of critical cross-slip parameters is the main contribution of the thesis. The criterion discussed in Section 2.5 is based in Brown's work [20]. Based on the criterion we can construct the graph of function $\tau_{app}(h)$ shown in Fig. 12 (nickel at room temperature), which represents the condition $\tau_{cs} = \tau_p$. For values h and τ_{app} above the graph in the (h, τ_{app}) plane, the primary slip continues. For the values below, the cross-slip occurs.

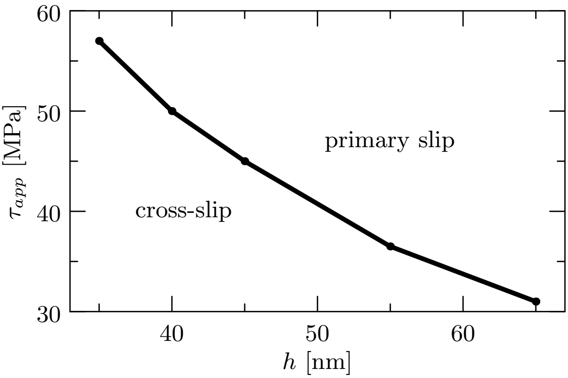

Figure 12: Graph of the cross-slip borderline $\tau_{cs}(h)$ for Ni (room temperature).

The applied stress needed for bypassing is called the passing stress τ_{pass}. The graph of $\tau_{pass}(h)$ can be constructed in a similar way. Let us consider the same arrangement of two dislocations of the opposite signs in η_1 and η_2 planes neglecting cross-slip. The approaching dislocations form either a dipole or bypass one another. We can construct a borderline $\tau_{pass}(h)$ of the lowest applied stress required for the passing of the dislocations in the parallel planes in the distance h apart as shown in Fig. 13 (nickel at room temperature).

Brown's criterion is illustrated in Fig. 14. In the (h, τ_{app}) plane, the graphs $\tau_{app}(h)$ and $\tau_{pass}(h)$ intersect each other and the plane is divided into three regions. For values of h and τ_{app} in the region below the graph of $\tau_{app}(h)$ the cross-slip leads to the annihilation of the screw segments. In the region above both graphs the dislocations pass one another. In the region between the graphs on the right hand side from the intersection C, the screw dipoles are formed. The minimum width of the screw dipoles is delimited by the critical annihilation distance y_s determined by the intersection C. The point C represents the sharp cut-off in the distribution of screw dislocation dipole widths observed by Mughrabi, Ackermann and Herz [28]. Accepting Brown's criterion, the stress corresponding to the intersection C may be interpreted as the saturation stress τ_{PSB}.

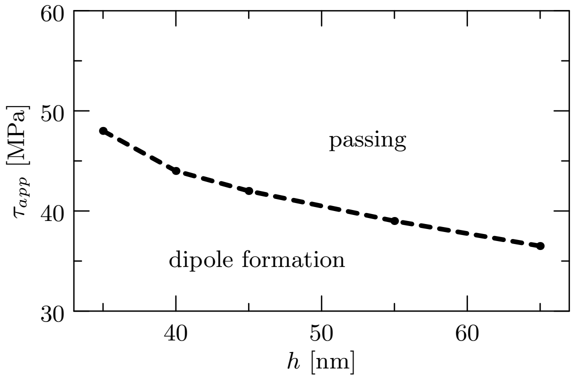

Figure 13: Graph of the passing borderline $\tau_{pass}(h)$ for Ni (room temperature).

In the formulation of the criterion, an ideal cross-slip geometry is considered, i.e. the cross-slip plane is geometrically defined as the unique plane connecting the screw segment parts gliding in two different primary glide planes. However, cross-slip can occur in many parallel planes before or after this special cross-slip plane, in general. In the cross-slip planes, the resolved shear stress reaches maximum provided the screw parts are nearly above each other forming a dipole. The annihilation of the screw dislocations along the parallel planes would require a double cross-slip into a common primary plane. If this annihilation process is energetically more favorable than the ideal cross-slip, annihilation has to be checked by a further simulation analysis of the whole process.

The graph of cross-slip $\tau_{app}(h)$ is determined as follows. For the fixed primary slip planes distance h, several simulations with different values of applied stress are performed to approximate the condition $\tau_{cs} = \tau_p$ as close as possible. This provides the value of $\tau_{appl}(h)$. Repeating the procedure for different h, the graph of $\tau_{app}(h)$ is obtained. The example is shown in Fig. 12. The graph of $\tau_{pass}(h)$ shown in Fig. 13 is constructed in a similar way. The values of the critical annihilation distance y_{s} and the saturation stress τ_{PSB} are determined by the intersection C of the graphs. The results for copper and nickel cycled at different temperatures and for silver at room temperature are listed in Table 3, Table 4 and Table 5 together with the available experimental data from [1, 13, 14, 22, 28, 52].

As some of the mentioned experimental data are scattered or estimated only, the sensitivity of the simulation results with respect to the input parameters is discussed. As noticed by Kwadjo and Brown in [20], the line tension is sensitive with respect to the value of Poisson's ratio ν. At the room temperature for copper, using $\nu = 0.4$ (see [6]) instead of $\nu = 0.34$ causes the change of τ_{PSB} from 29.5 MPa to 28.7 MPa. The critical annihilation distance y_{s} changes from 48 nm to 55 nm. For example the change of the friction stress from 4 to 5 MPa in the case of the room temperature copper causes the change of the predicted value of the saturation stress τ_{PSB} from

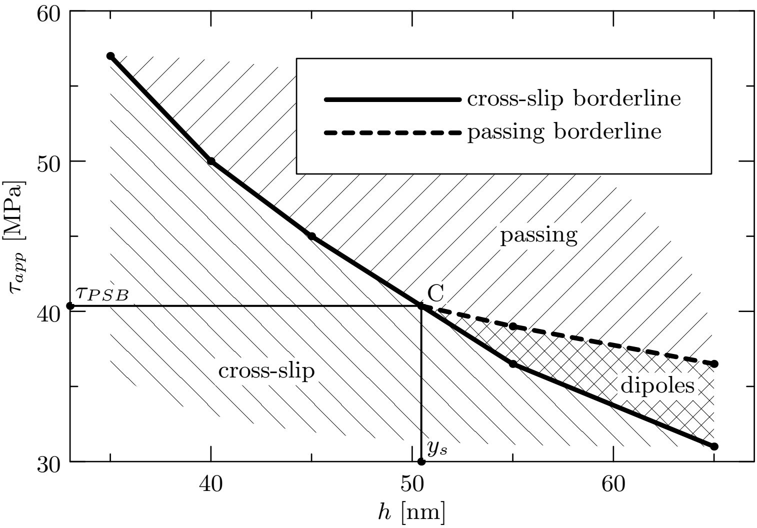

Figure 14: Graph of values y_s and τ_{PSB} for Ni at room temperature represented by the intersection C. The solid line is the graph of the cross-slip borderline $\tau_{app}(h)$, the dashed line represents the passing borderline $\tau_{pass}(h)$.

29 MPa to 31 MPa and of the critical annihilation distance y_s from 48 nm to 45 nm. The change of the wall distance from 1200 nm to 1300 nm for the room temperature copper leads to the change of τ_{PSB} from 29 MPa to 27 MPa and of y_s from 48 nm to 51 nm.

The agreement between the measured an predicted values presented in Tables 3, 4 and 5 indicates that the introduced simplifications (neglecting the dislocation core extension and the crucial role of the force balance at the screw tips reaching the cross-slip geometry for initiation of a cross-slip annihilation) are acceptable for the modeling at meso-scale.

The results summarized in Tables 3, 4, and 5 provide a hint for answers to the questions that are still not resolved in material science:

- what mechanism controls the critical cross-slip annihilation distance y_s;
- what mechanisms controls the saturation stress τ_{PSB};
- whether the Brown's criterion is a promising working hypothesis.

Brown's criterion manifests the controlling mechanism of the initiation of cross-slip annihilation confirmed by satisfactory agreement of the predicted values for copper, nickel and silver crystals with the available experiments.

At the meso-scale Tables 3, 4 and 5 seem to give the answer "cautious yes" to the question, whether the extension of the dislocation cores can be neglected and cross-slip treated as a deterministic, mechanically activated process. The results exhibit the

temperature	G	channel width	τ_{fr}	τ_{PSB}^{ex}	y_{s}^{ex}	τ_{ePSB}	y_{s}
[K]	[GPa]	[nm]	[MPa]	[MPa]	[nm]	[MPa]	[nm]
4	46	450	9	85	-	77	23
77	45	700	7	60-57	-	51	33
190	44	1050	5	39	-	35	43
295	42	1200	4	27-30	50	29	48
430	40	2140	3	19	-	18	69

Table 3: Experimental results τ_{PSB}^{ex}, y_{s}^{ex} [1, 13, 14, 28] and simulation results τ_{PSB}, y_{s} for copper.

temperature	G	channel width	τ_{fr}	τ_{PSB}^{ex}	y_{s}^{ex}	τ_{PSB}	y_{s}
[K]	[GPa]	[nm]	[MPa]	[MPa]	[nm]	[MPa]	[nm]
77	68	600	7	100	-	82	29
293	63	1200	4	50	-	41	51
600	53	3000	2	20	-	19	83
750	49	6100	1	9–14	-	12	116

Table 4: Experimental results τ_{PSB}^{ex} [52] and simulation results τ_{PSB}, y_{s} for nickel.

systematic deviations at low temperatures; the measured values of the saturation stress τ_{PSB}^{ex} are higher than the values τ_{PSB} predicted by the model. A possible explanation is that the activation energy needed for constriction is small enough to be supplied at higher temperatures but not at low temperatures. To overcome this barrier an additional applied stress is needed at the low temperatures. Unfortunately, the role of the stacking fault, the dislocation core extension, and its possible constriction as coming from the atomistic simulations is not clear at present.

There is one more important question that is still pending for answer. Why the scaled saturation stresses for copper, nickel and silver are almost the same. The answer to this question follows from the fact that the model is based just on two ingredients (besides the friction stress): the elastic moduli and the size of the dislocation pattern (the PSB channel width). The reason is that the PSB channel width for copper, nickel and silver at room temperature are roughly the same, $\approx 1.2\ \mu$m, the difference is only in the shear modulus G and the forces are of an linear elastic nature, hence, for the scaled saturation stresses the scaling by G gives the same value.

It is still unknown what mechanism controls the temperature dependence of the saturation stress. The model does not suggest any controlling mechanism. It is only demonstrated that the temperature dependence of the saturation stress and the cross-slip annihilation distance can be evaluated from the temperature dependence of the measured distance between the PSB wall and the temperature dependence of the elastic constants. According to the model, one would have to specify the mechanisms governing the temperature dependence of the PSB channel width.

The model raises a related question. The model proves that one of the main ingredients controlling the critical cross-slip annihilation distance y_{s} is the characteristic size

temperature	G	channel width	τ_{fr}	τ_{PSB}^{ex}	y_{s}^{ex}	τ_{PSB}	y_{s}
[K]	[GPa]	[nm]	[MPa]	[MPa]	[nm]	[MPa]	[nm]
293	26.2	1200	4	18	-	22	48

Table 5: Experimental results τ_{PSB}^{ex} [22] and simulation results τ_{PSB}, y_{s} for silver.

of the underlying dislocation pattern. The distance between the PSB walls controls the critical cross-slip annihilation distance through the dislocation curvature. This has been concluded by Essmann and Differt [13] and Brown [5] already. On the other hand, y_{s} is one of the basic parameters governing dislocation patterns. The cross-slip annihilation mechanism and the dislocation patterning are mutually related, and take part in a complex self organization process, which remains an open problem.

Summary

The dissertation thesis dealt with the discrete dislocation dynamics and the main focus was given to the topological changes (merging and splitting) and to the phenomenon of cross-slip. The work suggested and provided detailed description of the physical and mathematical model of the discrete dislocation dynamics which has been successfully applied to the phenomena occurring in metal crystals. The original results were in agreement with available experimental data. If the experimental data were not available, the model predicted their values (i.e., the critical cross-slip distance y_s).

A solid fundamentals of the dislocation theory and dislocation dynamics were presented in Chapter 1 in order to give all necessary information required to understand the presented model. The model described in the second part of Chapter 1 is based on the work of Kratochvíl and Sedláček [17] and its solution on the work of Minárik [25] and Křišťan [18], however, it is significantly improved. Topological changes achieved by an algorithm specifically developed for the discrete dislocation dynamics and the introduction of the cross-slip plane and the derivation of all active forces in the plane belong among the main contributions to the model.

Considering all requirements we eventually chose the parametric approach which can handle open and closed curves, is fast and accurate, and also well tested for the application in dislocation dynamics [3, 4, 18, 19, 24–26, 31, 33–36, 41–44]. The method was enriched by an algorithm for topological changes. The thesis paid special attention to the redistribution algorithm developed by Ševčovič and Yazaki [48–51] which is essential for the stability and accuracy of the numerical simulation. This aspect was ommited in this document.

In the thesis we compared a semi-discrete and semi-implicit scheme for the method of lines and a semi-implicit scheme for the finite volume method. Based on the EOC (estimated order of convergence), computation speed, and the suitability for the tangential redistribution we chose the finite volume method which is superior to the methods of lines (described in Section 3). We also dealt the tangential redistribution from the numerical point of view in detail and suggested the modification for the open curves which was not considered in the original work of Ševčovič and Yazaki [49].

The model was applied to several phenomena appearing in dislocation dynamics. The simulation of the Frank-Read source and the dislocation-precipitate interaction worked very well and provided qualitatively good results. However, this area of the dislocation dynamics deserves more attention and is a subject of the future research.

Main attention was paid to the simulation of two dislocations gliding in a PSB channel. The generalized model with the additional cross-slip allowed us to simulate the complete phenomenon of double cross-slip and annihilation of two screw dislocations by cross-slip. The estimation of the critical values for cross-slip using Brown's criterion is probably the biggest contribution of this work.

Let us sum up the results for the cross-slip simulation in several points.

- Cross-slip was treated as a deterministic, mechanically activated process. Based on *Brown's criterion* the proposed model predicted both the critical annihilation distance y_{s} and the saturation stress τ_{PSB} simultaneously and related them to the size of the dislocation pattern.

- The proposed cross-slip mechanism is governed by the line tension, the applied stress and the interaction force between dislocations of the opposite signs, which approach one another. The ingredients of the model are: the magnitude of the Burgers vector, the elastic moduli (appearing in the line tension and the interaction force), the friction stress, and the characteristic size of the dislocation pattern.

- The critical annihilation distance y_{s} is determined as the distance between the primary slip planes where the screw parts of the approaching dislocations are on a "cross-road". They are just on the point of the mutual annihilation exposed to the applied stress required to separate them. Such a value of the applied stress is interpreted as the saturation stress τ_{PSB}.

- The temperature dependence of τ_{PSB} and the corresponding critical annihilation distances y_{s} result from the temperature dependence of the elastic moduli and of the characteristic size of dislocation patterns.

- As presented in Tables 3, 4 and 5, the simulation results of y_{s}, τ_{PSB} are in good agreement with the available experimental data for copper, nickel, and silver single crystals.

The work touches several parts of the dislocation dynamics and provides answers, or at least hints, to the important questions of dislocation dynamics in general and cross-slip parameters in particular. There are, however, still many areas for the future research. The dislocation-precipitate interaction can be significantly improved by realistic simulation of precipitates. Dislocation loops generated by the Frank-Read mechanism should interact with each other and it should be possible to simulate the dislocation source for a longer time. Presented cross-slip model considers only the perfect cross-slip configuration (Fig. 6), however, the dislocations can switch the cross-slip plane before or after the perfect slip plane. Then the double cross-slip is required. Several simplifications, such as omitting the dislocation constriction, should be properly addressed.

Main results of this work will be published in upcoming papers [37–40].

References

[1] Z. S. Basinski and S. J. Basinski. The cyclic deformation of copper single crystals. *Progress in Materials Science*, 36:89–148, 1992.

[2] M. Beneš. Phase field model of microstructure growth in solidification of pure substances. *Acta Math. Univ. Comenian*, 70:123–151, 2001.

[3] M. Beneš, M. Kimura, P. Pauš, D. Ševčovič, T. Tsujikawa, and S. Yazaki. Application of a curvature adjusted method in image segmentation. *Bulletin of the Institute of Mathematics, Academia Sinica (New Series)*, 2008(4):509–523, 2008.

[4] M. Beneš, J. Kratochvíl, J. Křišťan, V. Minárik, and P. Pauš. A parametric simulation method for discrete dislocation dynamics. *The European Physical Journal ST*, 177(1):177–192, October 2009.

[5] L. M. Brown. Dislocation plasticity in persistent slip bands. *Mater. Sci. Eng.*, A 285:35–42, 2000.

[6] L. M. Brown. On the shape of a dislocation shear loop in stable equilibrium. *Philos. Mag. Lett.*, 81:617–621, 2001.

[7] L. M. Brown. A dipole model for the cross-slip of screw dislocations in fcc metals. *Philosophical Magazine A*, 82:1691–1711, 2002.

[8] K. Deckelnick and G. Dziuk. Mean curvature flow and related topics. *Frontiers in Numerical Analysis*, 1:63–108, 2002.

[9] B. Devincre. Three dimensional stress field expression for straight dislocation segments. *Solid State Communications*, 93 No. 11:875, 1995.

[10] K. Differt, U. Essmann, and H. Mughrabi. A model of extrusions and intrusions in fatigued metals II. Surface roughening by random irreversible slip. *Philosophical Magazine*, 54:237–258, 1986.

[11] G. Dziuk, A. Schmidt, A. Brillard, and C. Bandle. *Course on mean curvature flow.* Freiburg, 1994.

[12] C. L. Epstein and M. Gage. The curve shortening flow. In *Wave motion: theory, modelling, and computation*, California, 1986. Berkeley.

[13] U. Essmann and K. Differt. Dynamical model of the wall structure in persistent slip bands of fatigued metals II. The wall spacing and the temperature dependence of the yield stress in saturation. *Mater. Sci. Eng.*, A 208:56–68, 1996.

[14] U. Essmann and H. Mughrabi. Annihilation of dislocations during tensile and cyclic deformation and limits of dislocation densities. *Philosophical Magazine*, A40:731–756, 1979.

[15] F. C. Frank and W. T. Read Jr. Multiplication processes for slow moving dislocations. *Physical Review*, 79(4):722, 1950.

[16] J. Hirth and J. Lothe. *Theory of Dislocations.* John Willey, New York, 1982.

[17] J. Kratochvíl and R. Sedláček. Statistical foundation of continuum dislocation plasticity. *Physical Review B*, 77(13):134102, 2008.

[18] J. Křišťan and J. Kratochvíl. Interactions of glide dislocations in a channel of a persistent slip band. *Philosophical Magazine*, 87:4593–4613, 2007.

[19] J. Křišťan and J. Kratochvíl. Bowing out of dislocations from walls of persistent slip band. *International Journal of Materials Research*, 101:680–683, 2010.

[20] R. Kwadjo and L. M. Brown. Cyclic hardening of magnesium single crystals. *Acta Metall.*, 26:1117–1132, 1978.

[21] H. M. Ledbetter. Elastic constants of polycrystalline copper at low temperatures. Relationship to single-crystal elastic constants. *Physica Status Solidi (a)*, 66:477–484, 1981.

[22] P. Li, Z. F. Zhang, X. W. Li, S. X. Li, and Z. G. Wang. Effect of orientation on the cyclic deformation behavior of silver single crystals: Comparison with the behavior of cooper and nickel single crystals. *Acta Mater.*, 57:4845–4854, 2009.

[23] K. Mikula and D. Ševčovič. Computational and qualitative aspects of evolution of curves driven by curvature and external force. *Comput. Vis. Sci.*, 6:211–225, 2004.

[24] V. Minárik and J. Kratochvíl. Dislocation dynamics – analytical description of the interaction force between dipolar loops. *Kybernetika*, 43:841–854, 2007.

[25] V. Minárik, J. Kratochvíl, and K. Mikula. Numerical simulation of dislocation dynamics by means of parametric approach. In M. Beneš, J. Mikyška, and T. Oberhuber, editors, *Proceedings of the Czech Japanese Seminar in Applied Mathematics*, pages 128–138. Faculty of Nuclear Sciences and Physical Engineering, Czech Technical University in Prague, Prague, 2005, ISBN 80-01-03181-0.

[26] V. Minárik, J. Kratochvíl, K. Mikula, and M. Beneš. Numerical simulation of dislocation dynamics. In M. Feistauer, V. Dolejší, P. Knobloch, and K. Najzar, editors, *Numerical Mathematics and Advanced Applications, ENUMATH 2003 (peer reviewed proceedings)*, pages 631–641. Springer Verlag, 2004, ISBN 3-540-21460-7.

[27] H. Mughrabi. Dislocation wall and cell structures and long-range internal stresses in deformed metal crystals. *Acta metallurgica*, 31(9):1367–1379, 1983.

[28] H. Mughrabi, F. Ackermann, and K. Herz. Persistent slipbands in fatigued face-centered cubic metals. In J. Fong, editor, *Fatigue Mechanisms, Proceedings of an ASTM-NBS-NSF symposium, Kansas city, May 1978*, pages 69–105, 1979.

[29] T. Mura. *Micromechanics of Defects in Solids.* Kluwer Academic Publishers Group, Netherlands, 1987.

[30] S. Osher and R. P. Fedkiw. *Level set methods and dynamic implicit surfaces.* Springer, New York, 2003.

[31] P. Pauš. Numerical simulation of dislocation dynamics. In *MAGIA 2007*, volume 1, pages 45–52, Bratislava, 2007. Slovak University of Technology, Faculty of Civil Engineering.

[32] P. Pauš. *Mathematical Model of Interactions in Discrete Dislocation Dynamics.* PhD thesis, Czech Technical University in Prague, Faculty of Nuclear Sciences and Physical Engineering, 2013.

[33] P. Pauš and M. Beneš. Algorithm for topological changes of parametrically described curves. In *Algoritmy 2009 Proceedings of Contributed Papers and Posters*, pages 176–184, Bratislava, 2009. Slovak University of Technology, Faculty of Civil Engineering.

[34] P. Pauš and M. Beneš. Direct approach to mean-curvature flow with topological changes. *Kybernetika*, 45(4):591–604, 2009.

[35] P. Pauš and M. Beneš. Topological changes for parametric mean curvature flow. In *Proceedings of Algoritmy conference*, Podbanské, 2009.

[36] P. Pauš and M. Beneš. Dislocation-precipitate interaction in discrete dislocation dynamics. *COE Lecture Note*, 36:55–62, 2012.

[37] P. Pauš, M. Beneš, M. Kolář, and J. Kratochvíl. A dislocation dynamics analysis of the critical cross-slip annihilation distance and the cyclic saturation stress in fcc single crystals at different temperatures. *Acta Materialia*, 61(20):7917 – 7923, 2013.

[38] P. Pauš, M. Beneš, M. Kolář, and J. Kratochvíl. Simulation of mutual interaction of dynamically evolving dislocations. In preparation, 2013.

[39] P. Pauš, M. Beneš, and J. Kratochvíl. Discrete dislocation dynamics in interaction with obstacles and cross-slip. In preparation.

[40] P. Pauš, M. Beneš, and J. Kratochvíl. Mechanisms controlling the cyclic saturation stress and the critical cross-slip annihilation distance in copper single crystals. Accepted to Philosophical Magazine Letters.

[41] P. Pauš, M. Beneš, and J. Kratochvíl. Discrete dislocation dynamics and mean curvature flow. In *Proceedings of ENUMATH 2009, the 8th European Conference on Numerical Mathematics and Advanced Applications*, pages 115–123, Uppsala, Sweden, 2009.

[42] P. Pauš, M. Beneš, and J. Kratochvíl. Model of topological changes in discrete dislocation dynamics. In *MMM 2010, Multiscale Materials Modeling, Freiburg, 2010, Conference Proceedings*, pages 119–122, Stuttgart, 2010. Fraunhofer Verlag.

[43] P. Pauš, M. Beneš, and J. Kratochvíl. Simulation of dislocation cross-slip. *RIMS Kokyuroku Bessatsu*, 2011.

[44] P. Pauš, M. Beneš, and J. Kratochvíl. Simulation of dislocation annihilation by cross-slip. *Acta Physica Polonica A*, 122(3):509–511, 2012.

[45] M. Peach and J. S. Koehler. The forces exerted on dislocations and the stress fields produced by them. *Physical Review*, 1950.

[46] S. A. Sethian. *Level set methods and fast marching methods*. Cambridge University Press, Cambridge, 1999.

[47] D. Ševčovič. Qualitative and quantitative aspects of curvature driven flows of planar curves. In P. Kaplický and Š. Nečasová, editors, *Topics on Partial Differential Equations*, pages 55–119. Lecture Notes Vol. 2, Jindřich Nečas Center for Mathematical Modelling, Faculty of Mathematics and Physics, Charles University in Prague, MatFyzPress, Prague, 2007.

[48] D. Ševčovič and S. Yazaki. On a motion of plane curves with a curvature adjusted tangential velocity. In *Proceedings of Equadiff 2007*, 2007.

[49] D. Ševčovič and S. Yazaki. Curvature adjusted method for evolution of plane closed curves. *Japan Journal of Industrial and Applied Mathematics*, 28(3):413–442, 2011.

[50] D. Ševčovič and S. Yazaki. Evolution of plane curves with a curvature adjusted tangential velocity. *Japan Journal of Industrial and Applied Mathematics*, 28:413–442, 2011. 10.1007/s13160-011-0046-9.

[51] D. Ševčovič and S. Yazaki. Computational and qualitative aspects of motion of plane curves with a curvature adjusted tangential velocity. *Mathematical Methods in the Applied Sciences*, 2012.

[52] B. Tippelt, J. Bretschneider, and P. Hähner. The dislocation microstructure of cyclically deformed nicle single crystals at different temperatures. *physica status solidi (a)*, 163:11–26, 1997.

[53] A. Weidner and M. Sauzay. Experimental evolution of the slip irreversibility factor. *Key Engineering Materials*, 465:223–226, 2011.

Publications

Publications in impacted journals

- Pauš P., Kratochvíl J., and Beneš M., *Mechanisms controlling the cyclic saturation stress and the critical cross-slip annihilation distance in copper single crystals*, to appear in Philosophical Magazine Letters. Impact factor: 1.156.
- Pauš P., Kratochvíl J., and Beneš M., *A dislocation dynamics analysis of the critical cross-slip annihilation distance and the cyclic saturation stress in f.c.c. single crystals at different temperatures*, Acta Materialia 61, No. 20 (2013), pp. 7917–7923. Impact factor: 3.941.
- Pauš P., Beneš M., and Kratochvíl J., *Simulation of dislocation annihilation by cross-slip.* Acta Physica Polonica A, 122, No. 3 (2012), pp. 509–5011. Impact factor: 0.433.
- Beneš M., Kratochvíl J., Křišťan J., Minárik V., Pauš P., *A Parametric Simulation Method for Discrete Dislocation Dynamics*, European Physical Journal ST, Special Topics 177 (2009), pp. 177–192. Impact factor: 0.840.
- Pauš P. and Beneš M., *Direct approach to mean-curvature flow with topological changes*, Kybernetika Vol. 45 (2009), No. 4, pp. 591–604. Impact factor: 0.445. **Cited by:** (C_1), (C_2) (citations listed in Web of Science).

Publications in non-impacted refereed journals

- Pauš P., Beneš M., and Kratochvíl J., *Simulation of dislocation cross-slip.* RIMS Kokyuroku Bessatsu B35 (2012), Kyoto, Japan, pp. 23–30.
- Pauš P. and Beneš M., *Dislocation-Precipitate Interaction In Discrete Dislocation Dynamics.* COE Lecture Note, vol. 36. Faculty of Mathematics, Kyushu University Fukuoka, ISSN 1881-4042, pp. 55–62
- Beneš M., Kimura M., Pauš P., Ševčovič D., Tsujikawa T., and Yazaki S., *Application of a curvature adjusted method in image segmentation.* Bulletin of Inst. of Mathematics, Academia Sinica, Taipei, 2007, pp. 509–523. **Cited by:** (C_4).
- Pauš P., *Computer Analysis of Fractal Sets.* Proceedings of Czech Japanese Seminar in Applied Mathematics 2006, in COE Lecture Note, Vol. 6, Faculty of Mathematics, Kyushu University Fukuoka, 2007, ISSN 1881-4042, pp. 171–175.

Contributions in books resulting from conferences

- Pauš P., Beneš M., and Kratochvíl J., *Discrete Dislocation Dynamics and Mean Curvature Flow.* In Numerical Mathematics and Advanced Applications, Proceedings of ENUMATH 2009, the 8th European Conference on Numerical Mathematics and Advanced Applications, Uppsala, Sweden. Kreiss, G.; Lötstedt, P.; Malqvist, A.; Neytcheva, M. (Eds.), ISBN: 978-3-642-11794-7, pp. 721–728. **Cited by:** (C_1), (C_2) (citations listed in Web of Science).

Contributions in proceedings

- Pauš P., Beneš M., and Kratochvíl J., *Model of Topological Changes in Discrete Dislocation Dynamics.* MMM 2010, Multiscale Materials Modeling, Freiburg, 2010, Conference Proceedings, Eds. Gumbsch P. and van der Giessen E. Fraunhofer Verlag, pp. 119–122, ISBN 978-3-8396-0166-2.
- Pauš P. and Beneš M., *Algorithm for topological changes of parametrically described curves*, in Algoritmy 2009, Proceedings of contributed papers and posters, ed. Handlovičová A., Frolkovič P., Mikula K. and Ševčovič D. Slovak University of Technology in Bratislava, Publishing House of STU, 2009, pp. 176–184, ISBN 978-80-227-3032-7. ISI listed. **Cited by:** (C_3).
- Beneš M., Minárik M., Pauš P., and Čulík Z., *Moving Boundaries in Material Science.* in DMHF2007: COE Conference on the Development of Mathematics with High Functionality, Book of Abstracts, Eds. M.T. Nakao, Faculty of Mathematics, Kyushu University, Fukuoka, October 2007, pp. 61–64.
- Pauš P., *Numerical Simulation of Dislocation Dynamics.* Magia, 2007 - Mathematics, Geometry and Their Applications, ISBN 978-80-227-2796-9, pp. 45–52.

Publications in preparation

- Pauš P., Beneš M., Kolář M., and Kratochvíl J., *Simulation of Mutual Interaction of Dynamically Evolving Dislocations.*
- Pauš P., Beneš M., and Kratochvíl J., *Discrete Dislocation Dynamics in Interaction with Obstacles and Cross-Slip.*

Citing references

(C_1) Ševčovič, D. and Yazaki, S., *Computational and qualitative aspects of motion of plane curves with a curvature adjusted tangential velocity.* Mathematical Methods in the Applied Aciences, 35(15) Special Issue, 2012, pp. 1784–1798.

(C_2) Ševčovič, D. and Yazaki, S., *Evolution of plane curves with a curvature adjusted tangential velocity.* Japan Journal of Industrial and Applied Mathematics, 28(3), 2011, pp. 413–442.

(C_3) Balažovjech M., Mikula K., Petrášová M., and Urbán J., *Lagrangean method with topological changes for numerical modelling of forest fire propagation.* In Proceedings of ALGORITMY 2012, pp. 42–52.

(C_4) Oberhuber T., Suzuki A., Vacata J., Žabka V., Image segmentation using CUDA implementations of the Runge-Kutta-Merson and GMRES methods, Journal of Math-for-Industry, 2011, vol. 3, pp. 73–79

Curriculum vitae

Personal data

- Name: Petr Pauš
- Address: Department of Mathematics
  Faculty of Nuclear Sciences and Physical Engineerings
  Czech Technical University in Prague
  Trojanova 13, Praha 2, 120 00
- Born: September 14, 1981
- Email: petr.paus@fjfi.cvut.cz

Education

- 2006 to present: Czech Technical University in Prague
  Faculty of Nuclear Sciences and Physical Engineering
  Theses: Numerical simulation of dislocation dynamics
  PhD student

- 2001-2006: Czech Technical University in Prague
  Faculty of Nuclear Sciences and Physical Engineering
  Thesis: Computer Analysis of Fractal Sets
  Master degree (Ing.)

Languages

- Czech (native), English (fluent), Japanese (intermediate)

Teaching

- 2006 – 2008: Programming basics. (Základy programování)
- 2007 – 2008: Algorithmization, exercises. (Základy algoritmizace, cvičení)
- 2008–2013 Calculus, exercises. (Matematika 1, Matematika 2, cvičení)

Research support and fellowships

- GAČR - P108/12/1463 "Two scales discrete-continuum approach to dislocation dynamics",
- SGS11/161/OHK4/3T/14 "Pokročilé superpočítačové metody implementace matematických modelů",

- VZ MŠMT 6840770100 "Applied Mathematics in Technical and Physical Sciences",
- LC06052 "Nečas Center for Mathematical Modelling" of the Ministry of Education, Youth and Sport of the Czech Republic.
- IGS ČVUT 2008, No. CTU0803714.

Conferences and workshops

- Pauš P., Beneš M., and Kratochvíl J., *Critical values for dislocation annihilation by cross-slip.* Workshop on Scientific Computing 2013, Děčín, Czech Republic, oral presentation.
- Pauš P., Beneš M., and Kratochvíl J., *Discrete dislocation dynamics.* Nečas Center for Mathematical Modeling, Prague, Czech Republic, May 6, 2013, oral presentation.
- Pauš P., *Dislocation annihilation by cross-slip.* Workshop on Scientific Computing 2012, Děčín, Czech Republic.
- Pauš P., Beneš M., and Kratochvíl J., *Dislocation annihilation by cross-slip.* Dislocations 2012, Budapest, Hungary, August 27–31, 2012, oral presentation.
- Pauš P., *Dislocation cross-slip with annihilation.* Workshop on Scientific Computing 2011, Děčín, Czech Republic, oral presentation.
- Pauš P., Beneš M., and Kratochvíl J., *Dislocation annihilation by cross-slip.* ISPMA 12, Prague, Czech Republic, September 4–8, 2011, oral presentation.
- Pauš P., *Dislocation cross-slip with annihilation.* Mathematical and numerical analysis for interface motion arising in nonlinear phenomena 2011, Kyoto, Japan, July 12–14, 2011, oral presentation.
- Pauš P., Beneš M., and Kratochvíl J., *Model of topological changes in discrete dislocation dynamics.* MMM 2010, Freiburg, Germany, October 4–8, 2010, oral presentation.
- Pauš P., Beneš M., *Numerical simulation of dislocation dynamics.* Czech-Japanese Seminar in Applied Mathematics 2010, Telč, Czech Republic, August 27–31, 2010, poster.
- Pauš P., *Discrete dislocation dynamics.* Workshop on Scientific Computing 2010, Děčín, Czech Republic, oral presentation.
- Pauš P., *Numerical simulation of dislocation dynamics.* ENUMATH 2009, Uppsala, Sweden, June 29 – July 3, 2009, oral presentation.
- Pauš P., *Algorithm for Topological Changes of Parametric Curves.* Algoritmy 2009, Podbanské, Slovak Republic, March 15–20, 2009, oral presentation.

- Pauš P., Beneš M., and Kimura M., *Comparison of Methods for Mean Curvature Flow* . Algoritmy 2009, Podbanské, Slovak Republic, March 15–20, 2009, poster.
- Pauš P. and Beneš M., *Direct approach to mean-curvature flow with topological changes.* Czech-Japanese Seminar in Applied Mathematics 2008, University of Miyazaki, Takachiho, Miyazaki, Japan, September 1–7, 2008, oral presentation.
- Pauš P., Beneš M., and Kimura M., *Comparison of Methods for Mean Curvature Flow.* Czech-Japanese Seminar in Applied Mathematics 2008, University of Miyazaki, Takachiho, Miyazaki, Japan, September 1–7, 2008, poster.
- Pauš P., *Numerical Simulation of Dislocation Dynamics* International workshop on fluid-structure interaction problems, Prague, Czech Republic, October 30 – November 2, 2007 oral presentation.
- Pauš P., *Numerical Simulation of Dislocation Dynamics* Mini workshop on pattern formation in reaction diffusion system with advection in Prague, Czech Republic, September 11–12, 2007, oral presentation.
- Pauš P., *Numerical Simulation of Dislocation Dynamics.* Slovak-Austrian Mathematical Congress, Podbanské, Slovak Republic, September 16–21, 2007, oral presentation.
- Pauš P., *Numerical Simulation of Dislocation Dynamics.* ICIAM 07, Zurich, Switzerland, July 15–20, 2007, poster.
- Pauš P., *Computer Analysis of Fractal Sets.* QNA Seminar, Fukuoka, Japan, October 31, 2006, oral presentation.
- Pauš P., *Computer Analysis of Fractal Sets.* Czech Japanese Seminar in Applied Mathematics 2006, Czech Technical University in Prague, September 14–16, 2006, Prague, Czech Republic, poster.

Research Stays

- August 2008, Hiroshima University, Hiroshima, Japan. 1 week.
- March 2008, Slovak Technical University, Bratislava, Slovak Republic. 1 week.
- January 2007, Slovak Technical University, Bratislava, Slovak Republic. 1 week.
- October 2006, Kyushu University, Fukuoka, Japan. 2 weeks.

FNSPE Activities

- Promotion of the faculty (Den otevřených dveří).
- The week of physics (Fyzikální týden).
- Faculty evaluation survey administration.